



Effects of Si/Al ratio on the interaction of nonthermal plasma and Ag/HY catalysts



Hyun-Ha Kim*, Yoshiyuki Teramoto, Taizo Sano, Nobuaki Negishi, Atsushi Ogata

National Institute of Advanced Industrial Science and Technology (AIST), 16-1 Onogawa, Tsukuba, Ibaraki 305-8569, Japan

ARTICLE INFO

Article history:

Received 29 August 2014

Received in revised form 10 October 2014

Accepted 3 November 2014

Available online 13 November 2014

Keywords:

Zeolite

Nonthermal plasma

Si/Al ratio

VOC removal

Plasma-induced fluorescence

ABSTRACT

The effect of the silica and alumina ratio (Si/Al) in HY was studied as an important parameter that determines the catalytic activity of zeolite under plasma activation. The Ag loaded on HY was in a more oxidized state at lower Si/Al ratios and in a more metallic state at higher Si/Al ratios. A substantial drop in the relative electrical resistivity occurred when Ag was supported on the HY at a Si/Al ratio of 40. A strong relationship between the propagation of surface streamers and the catalytic activity was observed when the Si/Al ratio was changed in the following order: $2.6 > 15 > 40$. The interactions of oxygen plasma and Ag-loaded HY zeolites were clearly demonstrated via electron spin resonance (ESR) measurements of divalent silver (Ag^{2+}) and Fe^{3+} cations and plasma-induced fluorescence of Ag-cation clusters.

© 2014 Elsevier B.V. All rights reserved.

1. Introduction

The combination of nonthermal plasma (NTP) and catalyst is currently attracting attention as a method for removing various pollutants such as NO_x , odors, and volatile organic compounds (VOCs) [1–5]. Various metal-supported catalysts (e.g., TiO_2 , $\gamma\text{-Al}_2\text{O}_3$, SiO_2 , CeO_2 , MnO_x , ZrO_2 , LaCoO_3 , and zeolites) have been tested, and found to be effective in terms of removal efficiency, selectivity toward CO_2 , and carbon balance [6–9]. One of the interesting phenomena that occurs in single-stage plasma-driven catalysis (PDC) is the highly oxygen-content dependent behavior of VOC decomposition. The authors initially reported a substantial increase in both the removal efficiency of VOC and CO_2 selectivity with increasing oxygen content in the gas mixture. We incorporated this strong oxygen-dependent behavior into a cycled system that consisted of two steps: adsorption and subsequent decomposition of adsorbed VOCs using oxygen plasma [10–12]. Recently, the cycled system was applied to the removal of benzene [13,14], toluene [15,16], and HCHO [17] using various adsorbent/catalyst combinations. It is essential that the materials in the cycled system have a large adsorption capacity and high catalytic activity under oxygen plasma. Activated carbon, which is a well-known and widely used adsorbent, was not considered for the cycled system because it is a highly conductive material with an electrical

resistivity of $\sim 10^{-1} \Omega \text{ cm}$ [18]. If only the catalytic activity under oxygen plasma is guaranteed, zeolites have the potential to be good materials for the cycled system.

Zeolites are crystalline aluminosilicates, which have characteristic micropores, cavities and channels according to their frame structures. The sizes of the micropores range from 3 to 20 Å and are comparable to the size of small molecules. The size-selective screening properties of zeolites, which are often referred to as molecular sieve, can enable selective removal of certain gas molecules from mixtures. According to the International Zeolite Association, 218 types of zeolites (framework-type codes) have been assigned as of July 2014 [19]. The number of studies focused on combining plasmas with zeolites is increasing constantly. Combined systems of NTPs with various zeolites have been examined for the removal of benzene [20], toluene [21–23], and xylene [24] and methane conversion [25–28]. However, the mechanism of the interaction remains elusive and further collection of data is necessary for a better understanding of how plasmas can activate zeolites. The fundamental structure of zeolites comprises a three-dimensional network of $(\text{AlO}_4)^{5-}$ and $(\text{SiO}_4)^{2-}$ moieties, which are linked to each other via oxygen atoms. As the relative amount of Al increases, the total charge becomes more negative and charge compensation cations are necessary to stabilize the structure. These cations play important roles in determining the zeolite properties such as adsorption capacity, hydrophobicity, ion exchange, and catalytic activity [29]. In contrast, as the Si/Al ratio increases, zeolites become more thermally stable, acid resistant and have a higher total surface acidity [30].

* Corresponding author.

E-mail address: hyun-ha.kim@aist.go.jp (H.-H. Kim).

In this work, we focused on the ratio of silica (Si) and alumina (Al), which are the two main constituents of the zeolite framework. Silver-loaded HY zeolites with Si/Al ratios ranging from 2.6 to 40 were prepared using conventional impregnation method. The effect of the Si/Al ratio on the catalytic activities of HY zeolites was evaluated with or without nonthermal plasma activation. Using the same framework structure (i.e., HY) limited the number of variables, which enabled elucidation of the catalytic properties that depend on the Si/Al ratio. We primarily focused on the characterization of the catalyst rather than the catalytic reaction. The plasma-induced surface species were measured using an X-band electron-spin resonance (ESR) spectrometer. The physical interaction of the nonthermal plasma and catalysts were studied using an optical lens and intensified charge-coupled device (ICCD) camera system. The correlation between plasma propagation and catalytic activity are also discussed based on the results.

2. Experimental

2.1. Preparation and characterization of catalyst

HY zeolites (faujasite) with different Si/Al ratios (i.e., 2.6, 15, and 40) were used in this study. The zeolite samples were extrudates with diameter of 1.6 mm and lengths of 2–5 mm. Silver was impregnated using a AgNO₃ (Wako Chemicals LTD, 99.8% purity) precursor, which was dissolved into deionized water with stirring. The resultant solution containing the desired amount of Ag (10 wt%) was added to a zeolite-filled round-bottom flask and held overnight at room temperature. After removing the water using a rotary evaporator, the zeolites were calcined for 10 h at 500 °C in air. The amounts of Ag on the zeolites after impregnation were quantitatively determined using inductively coupled plasma optical emission spectroscopy (ICP-OES, SII Nanotechnology Inc., Model 3520UV). The sizes and shapes of the loaded Ag particles were measured using transmission electron microscopy (TEM, Topcon Co. Model EM002B). The Brunauer–Emmett–Teller (BET) surface areas were determined via nitrogen adsorption at 77 K (BELSORP 28). Table 1 summarizes the properties of the zeolite used in this study. The colors of the Ag-supported HY zeolites differed according to the Si/Al ratios; Zeolites with Si/Al ratios of 2.6, 15, and 40 were white, light gray, and dark gray, respectively. These differences in colors indicated that the degree of reduction increased as the Si/Al ratio increased. Compared to intact HY zeolites, the Ag/HY had 15–19% smaller BET surface areas. The electrical resistivities of the Ag/HY catalysts were measured using a Keithley electrometer




(Model 6514) at room temperature. The surface morphology, pressure, and porosity could affect the electrical resistivity; therefore, the measurements were performed using zeolite pellets instead of sheets. The measurement of resistivity was reproducible within ±50%. From the perspective of practical applications, these data reflect the actual conditions in the plasma reactor rather than the physical properties of the material.

The prepared catalysts were analyzed using a powder X-ray diffractometer (Rigaku, Model MiniFlex II). A Cu-K α (λ = 1.54 Å) X-ray source (30 kV and 15 mA), step width of 0.02° (2 θ), and scan speed of 0.5°/min were employed for the measurements. X-ray photoelectron spectroscopy (XPS; Fisons Instruments, Escalab 220i-XL) with Al-K α radiation ($h\nu$ = 1486.6 eV) was also used to characterize the Ag catalysts supported on the HY zeolites. Electron-spin resonance (ESR) spectrometer (JEOL JES-TE300) was implemented to identify the surface species that were fixed on the zeolites by the oxygen-plasma treatment. The frequency and intensity of the microwaves were 9.17682 GHz and 10 mW, respectively. The test catalysts were packed in an ESR sample tube, purged with pure oxygen for 10 min, and then sealed with a silicon plug. A stainless steel wire was inserted into the tube as a high voltage electrode, and aluminum foil was wrapped around the tube as a ground electrode. Plasma (18 kV_{pk}, 300 Hz) was applied for 10 min at room temperature. The plasma-treated catalyst samples were set in a Dewar flask containing liquid nitrogen (77 K), which was placed in the ESR spectrometer. We also focused on the ESR signals of iron impurities (Fe³⁺) that are typically present in zeolites.

2.2. Catalytic performance

The catalytic performance under plasma application was measured at varying oxygen contents, with all other parameters held constant. The concentration of benzene was 200 ppm and the total flow rate was 5 L/min under standard conditions (0 °C, 1 atm). The gas flow rates were measured using mass-flow controllers (Kofloc Co. FCC-3000). Details on the experimental setup and procedure were previously reported [12]; therefore only brief overview of the pertinent features are provided here. A coil electrode (0.45 mm stainless steel wire) was placed on the inner surface of the quartz tube (inner diameter 10 mm, effective length 200 mm). The outer surface of the quartz tube was painted with silver paste, which served as the ground electrode. This configuration prevented parasitic discharge in the air gap between the dielectric material and ground electrode [31]. The concentrations of benzene and byproducts (i.e., CO, CO₂, formic acid) were measured using a

Table 1
Properties of HY zeolites.

Catalyst	HY-2.6	HY-15	HY-40
Si/Al	2.6	15	40
			
Shape	Pellet	Pellet	Pellet
Color (as prepared)	White	Light gray	Dark gray
Size	Ø1.6 mm × ~5 mm	Ø1.6 mm × ~5 mm	Ø1.6 mm × ~5 mm
Density	0.50 g/cm ³	0.51 g/cm ³	0.49 g/cm ³
Ag wt%	9.05	8.57	8.44
BET	648 (bare)	708 (bare)	730 (bare)
(m ² /g)	533 (with Ag)	605 (with Ag)	593 (with Ag)

Spectrum One (Perkin Elmer Inc.) Fourier-transform infrared (FTIR) spectrometer equipped with a long-path gas cell and deuterated triglycine sulfate (DTGS) detector.

The thermal activities of the catalysts toward the oxidation of 150 ppm benzene in the absence of plasma were also evaluated. Catalyst samples (1.6 ± 0.1 g.) were packed in a quartz tube (10 mm inner diameter), which was then placed in an electrical oven. A thermocouple was inserted at the bottom of catalyst bed to monitor the temperature. The catalytic activity toward ozone decomposition was also investigated using 0.5 g of catalyst in the temperature range up to 100°C . Ozone was generated by a dielectric barrier discharge (50 Hz, 11 kV) with pure oxygen at a rate of 1 L/min. The ozone concentration was measured using a UV absorption-type ozone monitor (Ebara, Model PG320).

2.3. Power measurement and plasma observation

Plasma propagation on the surface of zeolite was visualized using an ICCD camera (Hamamatsu Photonics; C9016-03, C8484-05G). Four optical lenses (Mitutoyo, M Plan Apo series) with different magnifications were attached to the revolver, and a $2\times$ lens was used in this study. A plate-to-plate type DBD reactor was used to observe plasma propagation on the surfaces of the HY zeolites. The DBD plasma reactor was placed on an XY stage. The images of the plasma were recorded using HiPic software (Ver 8.1).

All the plasma reactors used in this study were energized by an AC high voltage (50–1000 Hz frequency) using a function generator (Tektronix, AFG310) and Trek 20/20B amplifier. The applied voltage and discharge current were determined using a digital oscilloscope (Tektronix, Model TDS 3034B) with a high-voltage probe (Tektronix, 6101A) and current transformer (Pearson Electronics, Model 2877). Lissajous Figure software (Insight Co., Lissajous Ver 1.72) was used to measure the discharge power. The optical emission from the catalyst-packed plasma reactor was measured using an Acton Research Corporation SpectraPro-300i spectrometer.

3. Results

3.1. Catalyst characterization

The size distributions of silver nanoparticles on the HY zeolites are given in Fig. 1. The silver nanoparticles were evenly dispersed on the zeolites with mean diameters of 3.2 nm. The Ag amounts on the zeolites, as measured using ICP (see Table 1), decreased in the following order of Si/Al ratios: $2.6 > 15 > 40$. These results were rationalized by the fact that Ag ions were incorporated into the micropores or framework of the zeolite via ion-exchange [32].

Fig. 2 shows the XRD patterns of the Ag/HY zeolites. Despite the Ag loading of ~ 10 wt%, the X-ray diffractograms were similar to that of intact HY zeolites indicating no significant modification of the frame structure. It was difficult to discuss the speciation of Ag from the XRD spectra because the most prominent diffraction peak of Ag_2O ($2\theta = 32.8$) overlapped with a strong peak of the intact HY zeolites. A weak peak corresponding to Ag ($2\theta = 38.1$) was evident for the zeolite with a Si/Al ratio of 40, but not for the other two Ag/HY zeolites.

Fig. 3 shows the narrow scan XPS spectra of the Ag3d region of the Ag-impregnated zeolites. The binding energies of Ag 3d for metallic Ag and Ag oxide (Ag_2O) only differ by ~ 0.5 eV, which usually makes it difficult to assign the measured peaks of Ag. The difference of the binding energies (ΔBE) of the Ag $3d_{5/2}$ and Ag $3d_{3/2}$ peaks (i.e., 367.7 and 373.7 eV, respectively) was 6.0 eV, which was consistent with the ΔBE for metallic Ag and Ag oxide [33]. The measured full width at half maximum (FWHM) was about 2.4 eV, which was slightly larger than those in the spectra of pure Ag (> 1.2 eV)

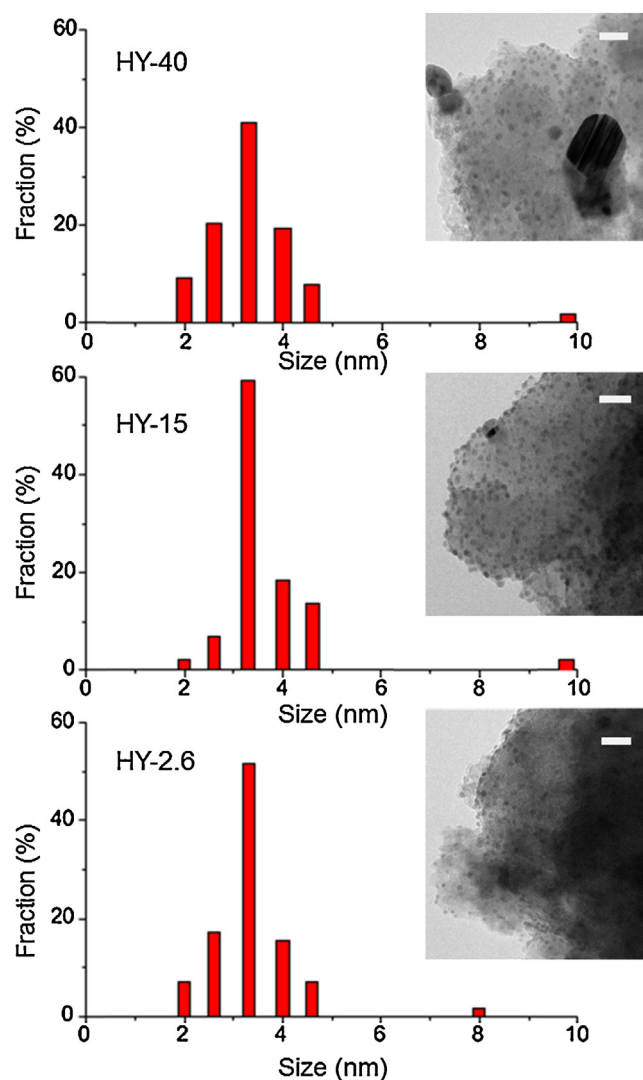


Fig. 1. Size distribution of Ag nanoparticles on HY zeolites. The scale bars in the TEM images correspond to 20 nm.

[34] and Ag_2O (> 1.8 eV) [35]. Thus, we concluded that several peaks corresponding to different states of Ag were superimposed in the measured spectra. Although the peak convolution was not sufficient to clearly discern the Ag species, all three samples contained the Ag $3d_{5/2}$ peak at 368.2 eV, which was assigned to metallic Ag [36,37]. The BE of Ag $3d_{5/2}$ for Ag/HY-2.6 was 367.5 eV, which was 0.2 eV lower than those of Ag/HY-15 and Ag/HY-40 (367.7 eV). This negative shift in the BE of Ag/HY-2.6 indicated that the Ag on HY-2.6 was in a more oxidized state than that in the other two samples [38]. Kang et al. also reported the coexistence of monovalent Ag ions and metallic Ag on a Ag/CeO_2 catalyst for CO oxidation [39]. Most elements in a positive ionic state exhibit a positive shift of the EB toward a higher energy. Ag is an exception to this trend. The BE of Ag 3d tends to shift to a lower energy as it is oxidized [40].

3.2. Evaluation of catalytic performance without plasma

Fig. 4 shows the thermal catalysis of 150 ppm benzene over the Ag/HY zeolites in the absence of plasma. The light-off temperature was 200°C for the HY with Si/Al 40, which exhibited the highest catalytic activity. The catalytic performances increased in the order of ascending Si/Al ratio in the zeolites: HY-40 > HY-15 > HY-2.6. It has been reported by many research groups that the catalytic

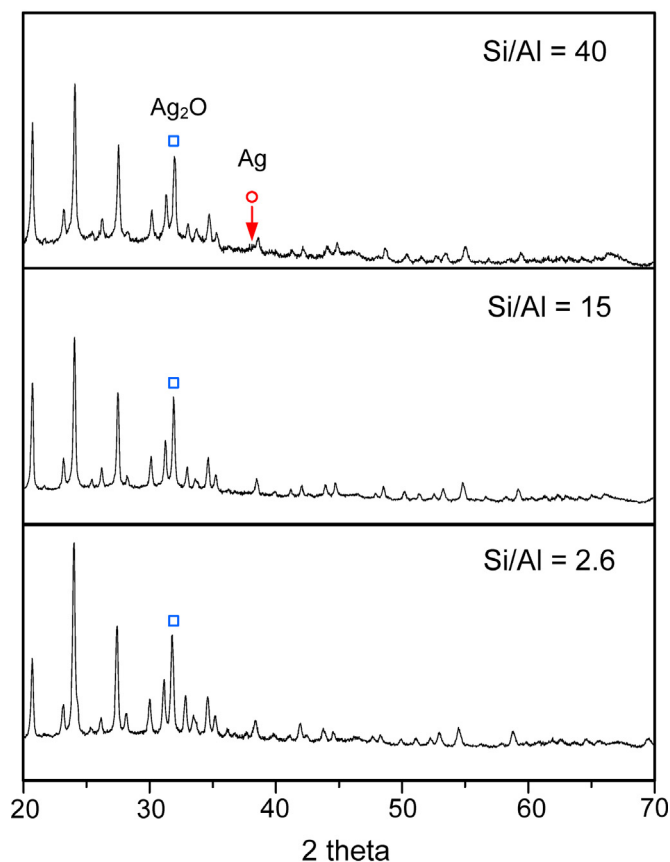


Fig. 2. XRD patterns of Ag/HY zeolites.

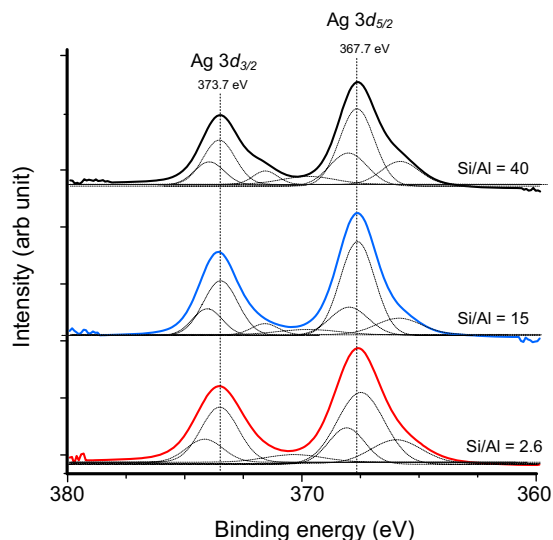


Fig. 3. XPS spectra of the Ag-supported HY zeolites (a) Ag 3d.

performance depends on the oxidation state of Ag; the effect that Ag has depends on the type of reaction. For example, Baek et al. reported that metallic Ag played an important role in toluene oxidation over a Ag/HY catalyst [41]. They also indicated that ion-exchanged Ag (Ag^+ , isolated ions in the zeolite support) showed poor activity. Corro et al. compared the catalytic behaviors of Ag, Cu, and Au for soot oxidation and reported that the metallic Ag-supported SiO_2 catalysts exhibited the highest activity [42]. In contrast, Nanba et al. studied the decomposition of acrylonitrile (AN) over Ag (5 wt%) with seven different supports (i.e., ZSM-5,

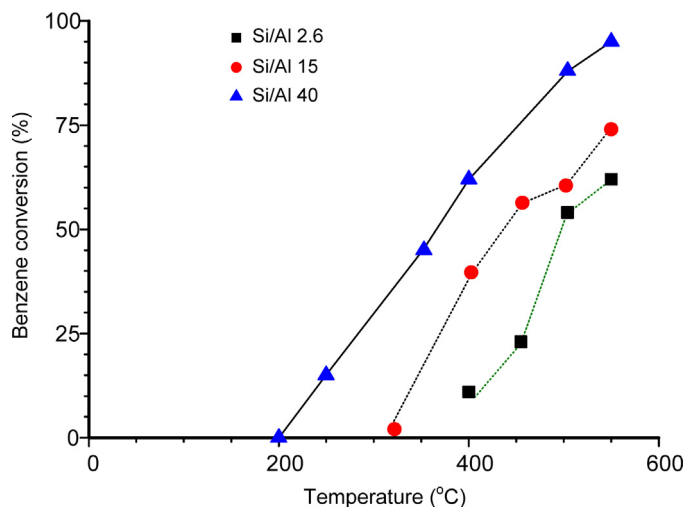


Fig. 4. Thermal catalysis of 150 ppm benzene over Ag-impregnated HY zeolites in synthetic air (without nonthermal plasma). Total flow rate was 1 L/min. The amount of catalyst was 1.6 ± 0.1 g.

Al_2O_3 , TiO_2 , SiO_2 , MgO , ZrO_2 , and TiO_2) and concluded that the presence of both oxidized and metallic Ag species was important for AN decomposition [43]. Oxidized Ag promoted the hydrolysis of AN to NH_3 , and metallic Ag enhanced the subsequent oxidation of NH_3 to N_2 .

The catalytic performances for ozone decomposition were also determined because plasma always produces ozone, which can decompose on the surface of catalysts to form active oxygen species. Fig. 5(a) and (b) shows the catalytic performances for ozone decomposition over bare HY and Ag/HY zeolites, respectively. Ozone was generated by an O_2 -fed ozonizer (surface barrier discharge) and injected into a catalyst bed containing 0.5 g of catalyst. In the case of the bare HY zeolites, ozone decomposition occurred at 100°C and the activity decreased in the following order of Si/Al ratios: $40 > 2.6 > 15$. No ozone decomposition occurred at temperatures below 50°C , and adsorption of ozone reached saturation within about 25 min. When Ag was present on the HY zeolites, ozone decomposition occurred even at room temperature. This observation suggested that the Ag played a major role in the activities of the catalysts toward low-temperature ozone decomposition. Aside from the differences in the decomposition rate of ozone with or without Ag-loading, the catalytic performance decreased in the same order of Si/Al ratios: $40 > 2.6 > 15$. Similar results have been reported for zeolites (H-MCM) with relatively high Si/Al ratios (>20); for example, a Si/Al ratio of 50 resulted in higher ozone decomposition than a Si/Al ratio of 20 at 296 K [44]. Silica MFI (ZSM5) was also found to be effective for ozone decomposition resulting in enhanced toluene oxidation [45]. A similar result was also reported for water treatment, where a high Si/Al ratio was essential for the adsorption of water-dissolved pollutants on zeolites [46]. Fujita et al. studied the ozone-induced decomposition of TCE over two zeolites (i.e., ZSM-5 and MOR) with different Si/Al ratios [47]. They found that TCE conversion increased with increasing Si/Al ratio and became saturated above a Si/Al ratio of 15. Ozone decomposition over Ag/HY suggested that metallic Ag was more active than the Ag oxide and that the exchanged Ag^+ ions also contributed, but to a lesser extent.

3.3. Relationship between surface streamers and the catalytic performance

The two key aspects required for a catalyst to be used in a cyclic system are adsorption capacity and catalytic performance

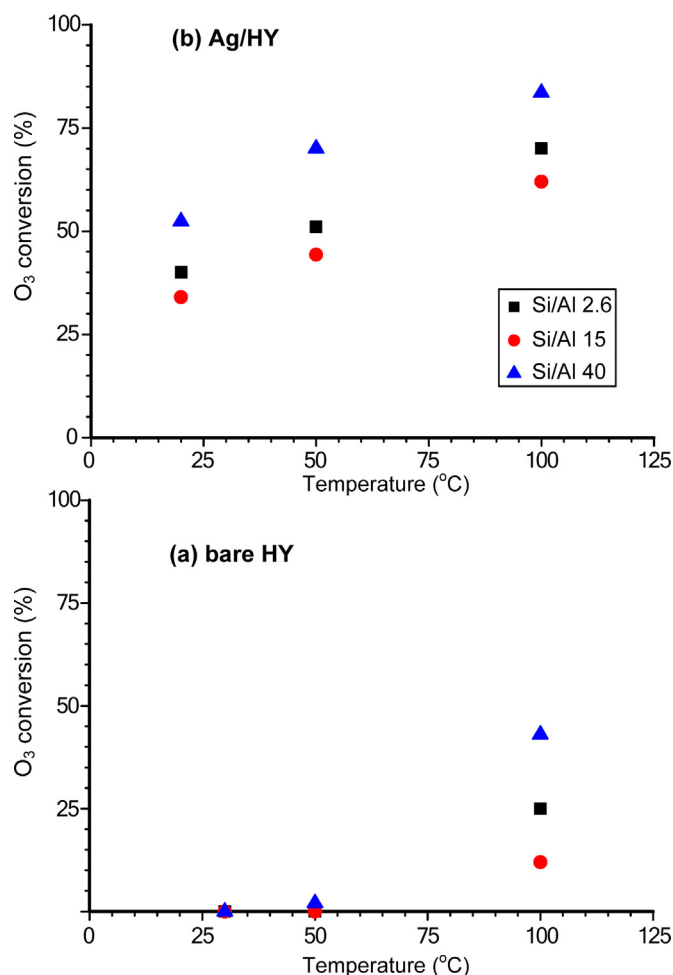


Fig. 5. Catalytic activity toward ozone decomposition: (a) Bare HY, and (b) Ag/HY zeolites. Ozone concentration was 1550 ppm. Gas flow rate was 1 L/min. The amount of catalyst was 0.5 g.

under oxygen plasma. The adsorption capacity was evaluated using 200 ppm benzene at 100 °C, and was found to be inversely proportion to the Si/Al ratio (in brackets): 55.4 mg/cm³-CAT (2.6) > 19.4 mg/cm³-CAT (30) > 16.8 mg/cm³-CAT (40). The oxygen content-dependent catalytic activity was evaluated using the enhancement factor (EF), which is a measure of the degree of enhancement of the decomposition removal efficiency (DRE) of VOCs with respect to the increase in oxygen content ([O₂] in%) of the gas mixture [12], as per the following equation.

$$EF = \frac{[DRE]_{\text{Oxygen}} - [DRE]_{\text{Air}}}{[O_2]_{\text{Oxygen}} - [O_2]_{\text{Air}}} \times 100 \quad (1)$$

Fig. 6 compares the catalytic activities of the Ag/HY zeolites in terms of the EF values. The results indicated that larger EF values resulted in higher catalytic activities as the oxygen content increased. The EF values were evaluated for the decomposition of 200 ppm benzene and decreased in the following order of Si/Al ratios: 2.6 > 15 > 40.

Fig. 7 shows the ICCD camera images of plasmas on the surfaces of Ag/HY zeolites. Plasma expansion over the surface of catalyst plays a crucial role in the decomposition of VOC using a PDC reactor [48]. As was indicated in previous studies [5,48], there are two types of discharge in a catalyst-packed plasma reactor. One is known as partial discharge, where numerous discharges occur at the contact points of the catalytic materials [49,50]. The partial discharges were explained by electric field augmentation, which was caused

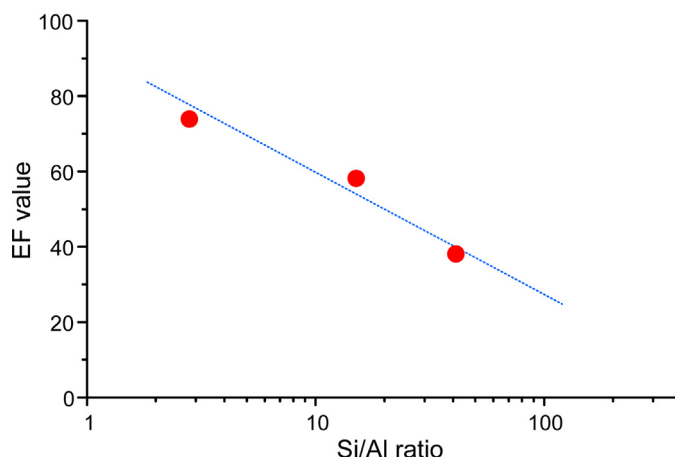


Fig. 6. Effect of Si/Al ratio in Ag/HY zeolites on the catalytic activity based on the enhancement factor (EF).

by the large dielectric constants of the packing materials [50–52]. The dielectric constants of zeolites change with the types and structures; however, typical values are in the range 1.5–5, i.e., larger than the air [53,54]. The second type of discharge is surface streamers. In the case of Ag/HY-2.6, the tracks of several surface streamers that propagated on the surface of the zeolites were evident. The numbers of streamers and their intensities decreased as the Si/Al ratio increased and the partial discharges became dominant in the HY-40 zeolite. It is also worth noting that the shapes of the surface streamer were affected by the Si/Al ratios. At a low Si/Al ratio (2.6), the surface streamers were more diffuse than those at higher Si/Al ratios. The diameters of the surface streamers were about 180–200 μm and 80–90 μm for the zeolite with the lowest Si/Al ratio (HY-2.6) and those with the higher Si/Al ratios (HY-15 and HY-40), respectively.

The loading of Ag could affect the electrical resistivity of a zeolite, which was expected to play an important role in the propagation of surface streamers. Fig. 8 compares the relative resistivity of Ag/HY and bare HY. The electrical resistivities of the bare HY zeolites were in the order of HY-2.6 ($1.5 \times 10^{10} \Omega \text{ cm}$) > HY-15 ($2.1 \times 10^9 \Omega \text{ cm}$) > HY-40 ($1.9 \times 10^9 \Omega \text{ cm}$); thus, it was evident that the loading of Ag decreased the electrical resistivity. The diminution of the relative resistivity became more significant as the Si/Al ratio increased. For HY-40, the relative resistivity decreased to 0.004. This observation clearly indicated that a conductive surface was unfavorable not only for the propagation of surface streamers but also for catalytic activity under oxygen plasma. Even in the same zeolite (HY), the Si/Al ratio altered the status of the supported metal and affected the propagation of surface streamers. These changes in the plasma properties were directly connected to the catalytic activity under plasma.

3.4. ESR evidence of the interaction between plasma and Ag-supported HY zeolites

To further elucidate the interactions of the plasma and catalysts we measured the O₂ plasma-treated Ag/HY zeolites using an ESR spectrometer. Fig. 9 shows the X-band ESR spectra of Ag/HY zeolites, which were treated with atmospheric-pressure O₂ plasma at room temperature. Signals were observed in the magnetic field ranges 200–400 mT for the Ag ion (Fig. 9(a)) and 105–205 mT for the Fe ion (Fig. 9(b)); their intensities were inversely proportional to the Si/Al ratio. The shapes of the ESR spectra in Fig. 9(a) were similar to that of the superoxide anion radical (O₂^{•−}); however, the measured g factors were clearly different from those for O₂^{•−} on Ag/Vycor quartz [55] and on BaY that was irradiated with X-rays or

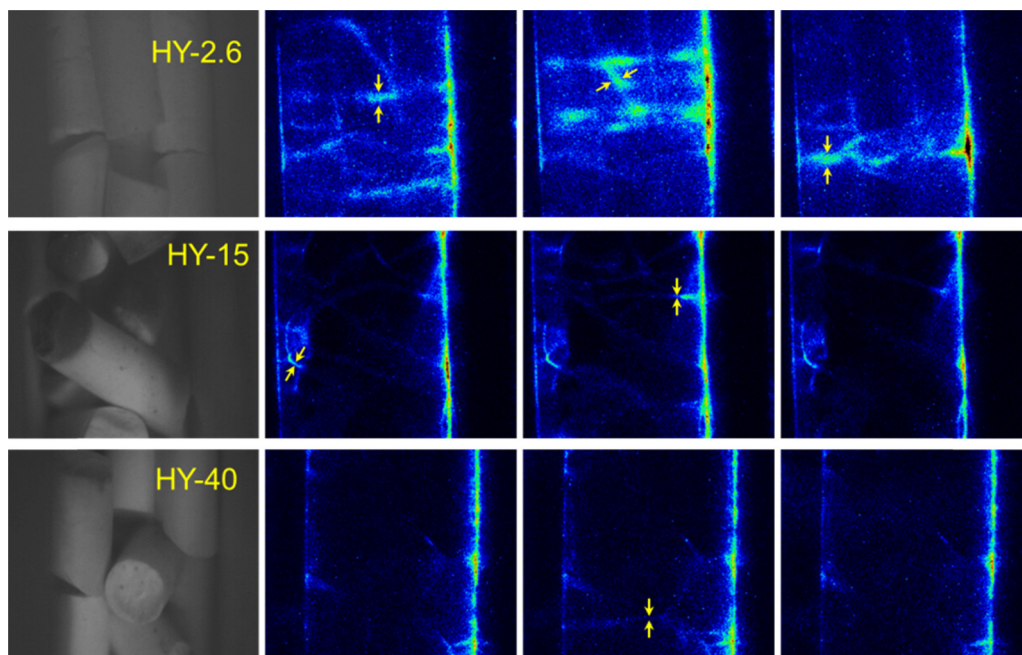


Fig. 7. ICCD camera images of plasma patterns in Ag-impregnated HY zeolites. The applied voltage and frequency were 30 kV_{pp} and 200 Hz, respectively. The gate time was 10 ms, which corresponded to two cycles of the applied voltage.

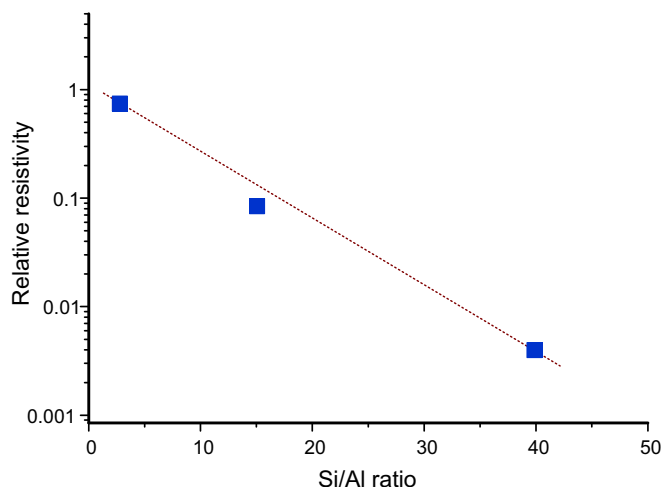


Fig. 8. Influence of the Si/Al ratio on the relative resistivities of the catalysts.

γ -rays [56]. The g factors were 2.26 and 2.03, which were assigned to divalent silver-ion clusters (Ag_n^{2+}). These values were consistent with those in previous works regarding Ag-supported faujasites: γ -ray irradiated Ag/X zeolite ($g_{11} = 2.250$, $g_{\perp} = 2.038$) [57] and Ag/NaY ($g_{11} = 2.260$, $g_{\perp} = 2.0381$) [58]. Although the g values were slightly different ($g_{11} = 2.307$, $g_{\perp} = 2.045$), the formation of silver cluster ions (Ag_2^{+} and Ag_3^{2+}) has also been identified in Linde-type A zeolite that was X-ray-irradiated at 77 K and annealed at 240 K [59].

Fe is a well-known impurity in zeolite frameworks, although it is present at very low concentrations (<500 ppm) [60,61]. The X-band ESR spectra ($g = 4.3$) in Fig. 9(b) clearly shows the Si/Al ratio-dependent behavior of Fe^{3+} ion formation on the plasma-treated HY zeolites. The Fe^{3+} peaks were most intense at a Si/Al ratio of 2.6 and decreased with increasing Si/Al ratio. The ESR spectra of Fe^{3+} also supported the plasma-induced oxidation of metal ions in the zeolite framework. Both of the peaks (Fe^{3+} and Ag^{2+} ions) could be detectable even after several months, keeping the plasma-treated catalysts inside the sample tubes at room temperature. The

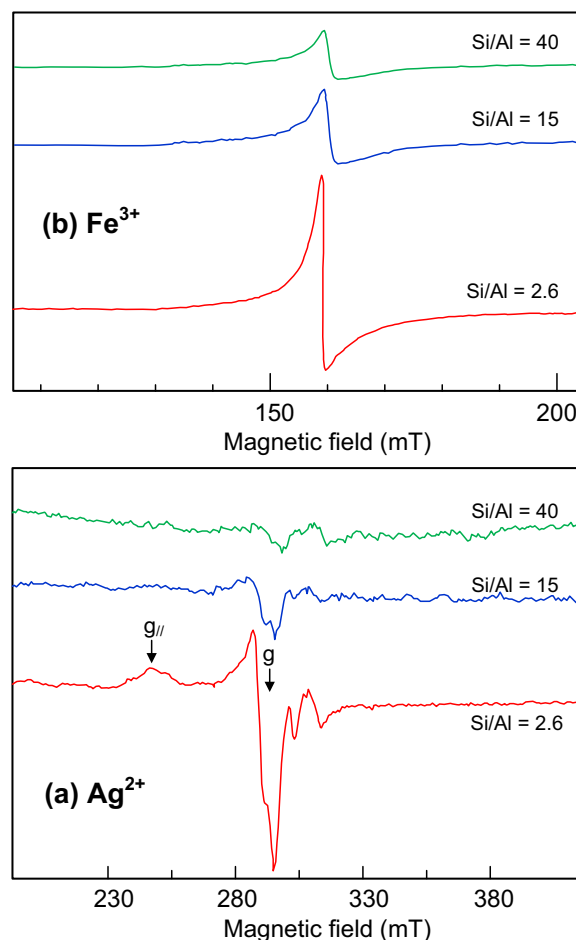


Fig. 9. ESR spectra of the O₂ plasma-treated zeolites.

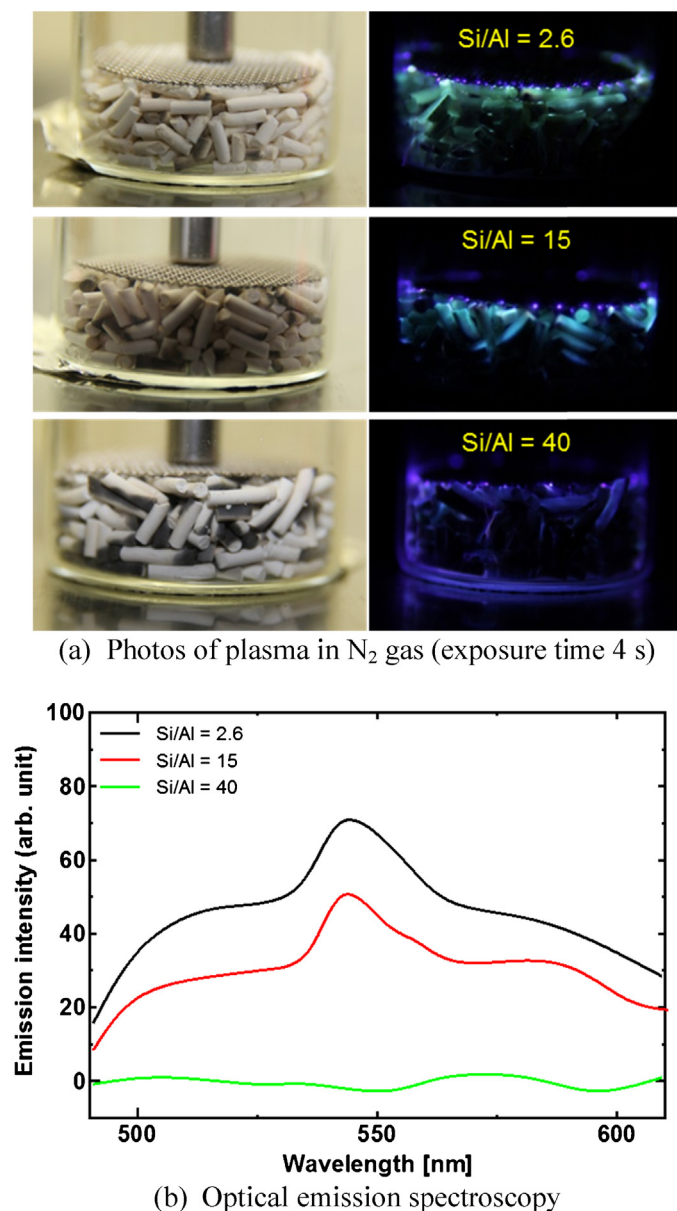


Fig. 10. Plasma-induced luminescence from the surface of Ag/HY zeolites: (a) Digital camera images of plasmas under N₂ gas flow, and (b) optical emission spectra under N₂ gas flow (AC high voltage with 50 Hz).

increased formation of Fe³⁺ and Ag²⁺ ions clearly correlated with the surface streamer propagation over the HY zeolites: increased propagation of the surface streamers resulted in increased ion formation because the interaction of plasma with the surface was essential to form these ions on the HY zeolite.

3.5. Plasma-induced fluorescence from the Ag/HY catalysts

Optical emission spectroscopy (OES) is a well-established non-intrusive diagnostic tool for plasma. OES can provide various insights into the fundamentals of plasma such as identification of short-lived radicals, electron energy distribution, and gas temperatures (rotation, vibration, and translation). However, the OES of plasma in the presence of catalysts has not been well investigated. Fig. 10(a) and (b) shows plasma images in N₂ and the plasma-induced fluorescence from the surface of Ag-supported HY zeolites, respectively. It is interesting to note that N₂ plasma in HY-2.6 exhibited a green color. The optical emissions of green were prominent

with at a Si/Al ratio of 2.6 and gradually changed to blue as the Si/Al ratio increased. Adsorption of benzene onto the Ag/HY zeolite gradually induced a color change from green to blue along the gas flow direction [62]. The emission converted from blue back to green as the adsorbed benzene was removed by oxygen plasma. The N₂ plasma can generate not only photons (i.e., UV light) but also energetic particles such as electrons, radicals, and excited metastable N₂ molecules. We also confirmed that UV irradiation instead of plasma could also induce similar fluorescence (data not given). However, it should be noted that visible light-induced photoluminescence required a high photon flux of 10–100 W/cm² [63,64], which was not possible from optical emission in plasma.

The green emission shown in Fig. 10(b) was found to be a broad spectrum with a peak wavelength at 542 nm. The peak intensities were in good agreement with the color change from green to blue. The emission pattern differed from the well-known gas-phase N₂ emission band, which suggested that the emission originated from the excited surface of the catalyst. In contrast to OES of plasma in gases or liquids, OES of plasma-induced fluorescence from the surface of a catalyst has not yet been studied. Instead, UV or visible light-induced luminescence has been studied for a variety of solid materials such as Ag⁺/ZSM-5 zeolite (excitation at 220 nm luminescence at 340 nm) [65] and CdS in NaY and MS-13X zeolites (excitation at 350 nm luminescence at 550 nm) [66]. The gas-phase reaction of unsupported Ag_xO clusters with ozone induced chemiluminescent emission at 500–600 nm [67]; therefore, the measured luminescence could be ascribed to the excited Ag clusters rather than the zeolite. Recently, Cremer et al. reported UV-induced fluorescence from heat-treated Ag-exchanged A, X and Y zeolites [63]. They also found that the UV wavelength for excitation and the resulting emission (550 nm) were dependent on the Si/Al ratio in faujasite zeolites such as Ag/NaX (Si/Al = 1.3) and Ag/NaY (Si/Al = 2.7) [63]. The intensities and wavelengths of the fluorescence were also influenced by a variety of factors such as excitation wavelength, type of zeolite, the presence of co-cations, and amount of Ag loading. They explained the fluorescence as the formation of excited Ag clusters within the zeolite framework.

4. Discussion

The single-stage plasma-driven catalysis of VOCs is generally studied below the light-off temperature, where the catalytic activity is not visible unless plasma is applied. To activate the catalyst under plasma, it is important to form the plasma adjacent to the surface of catalyst. As shown in Figs. 6 and 7, the catalysts that promoted the propagation of surface streamers exhibited higher catalytic activity; these results were consistent with our previous reports on metal nanoparticles (Ag or Cu)-supported zeolites (MS-13X, HY, MOR) [48]. Separate tests of catalytic activity toward O₃ decomposition (Fig. 5) indicated that ozone-induced oxidation was not the dominant mechanism on Ag/HY zeolites. The ESR spectra (Fig. 9) and OES of the catalyst (Fig. 10) suggested that oxygen plasma produced divalent Ag ions (Ag²⁺) as possible active sites on the surface of the Ag/HY with relatively low Si/Al ratios (<15). In O₂ plasma, atomic oxygen and ozone were the two most important species that played key roles in the oxidation of ion-exchanged Ag⁺ in the framework to form Ag_n²⁺ ion clusters.



Approximately 3–8 Ag atoms (Ag_n²⁺) were known to be incorporated into the zeolite framework [68]. Among them, a linear trimer Ag cluster, Ag⁺–Ag⁰–Ag⁺, has been suggested to be the most plausible Ag cluster in faujasite zeolite [33]. Comparison of O₃ conversion over the HY zeolites (Fig. 5) indicated that the O₃ reacted

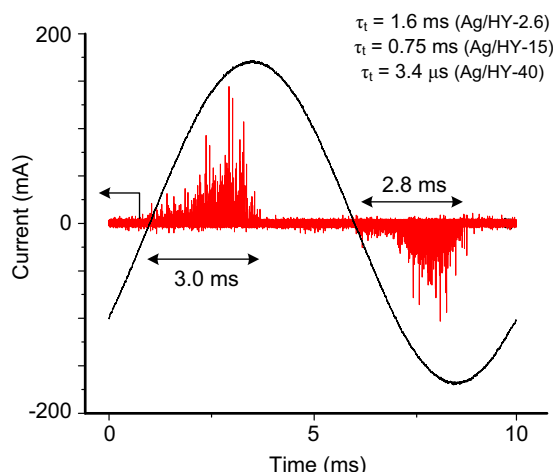


Fig. 11. Typical voltage-current waveforms of Ag/HY zeolites (frequency 100 Hz); τ_t in the figure indicates the charge relaxation time for each catalyst.

preferentially with metallic Ag nanoparticles, while direct oxidation by oxygen atoms appeared to be more responsible for the formation of Ag^{2+} and Fe^{3+} ions. The speciation of the surface oxygen species has yet to be unresolved, but there is experimental evidence for plasma-induced oxygen fixation on the surface of the catalyst. We previously reported the plasma-induced fixation of oxygen on Ag-supported TiO_2 and MS-13X using isotopically labeled oxygen ($^{18}\text{O}_2$) and on-line mass spectrometer [69]. The surface-fixed oxygen species can survive for up to 10 h [70].

Analysis of the Ag-supported HY zeolites indicated that the state of Ag on the HY zeolite had a significant impact on the catalytic activity under plasma activation. Ag-exchanged in the HY-2.6 framework was found to be beneficial for the expansion of surface streamers. However, the relative resistivity of Ag supported on HY-40 was reduced by a factor of 0.004. The large drop in resistivity could have shortened the charge relaxation time (τ_t) which was assumed to be detrimental to the propagation of surface streamer. τ_t was determined using the following equation:

$$\tau_t = \frac{\varepsilon_{\text{Cat}} \varepsilon_0}{K} \quad (2)$$

where ε_{Cat} is the dielectric constant of the catalyst, ε_0 is the permittivity of vacuum, and K is the conductivity. Fig. 11 shows waveforms of the applied voltage (15 kV_p) and discharge current at a frequency of 100 Hz. Discharges (i.e., current pulses) appeared over time periods of about 3.0 and 2.8 ms for the positive and negative half cycles of the voltage, respectively. Assuming that the ε_{Cat} value of the Ag/HY catalyst is 4, the τ_t for Ag/HY-2.6 was calculated to be 16 ms which is longer than the discharge period. However the short τ_t for Ag/HY-40 (3.4 μs) suggested that fast charge decay may have contributed to the poor propagation of the surface streamers for the HY zeolites with high Si/Al ratios.

The state of the Ag incorporated into the zeolites was not static but changed during the course of the catalytic reactions [71]. The Ag supported on HY zeolite may have undergone an intense oxidation/reduction reaction because of the plasma propagating on the surface. Silver oxide (Ag_2O) has a band gap of 1.3 ± 0.3 eV [35] and is known to readily undergo photoreduction to form metallic Ag clusters; the same could be said for the electrical resistivity. Plasma could have induced defects or oxygen vacancies on the surface of the catalyst [72], which tends to decrease the resistivity of the catalyst. Additionally, enhanced oxygen fixation by the plasma could have led to the increased resistivity. It was expected that these strong reduction-oxidation reactions of both metallic Ag and Ag cluster ions occurred under plasma activation, and the transient

state of Ag played a key role as an active site for the oxidation of VOCs.

In the case of catalyst preparation using glow plasma (low pressure), plasma treatment of catalysts tends to increase the dispersion of metal catalyst, catalytic activity, stability, and durability [73,74]. Although the reaction conditions differ from each other, the elementary processes are expected to have a lot in common. Further collections of experimental and theoretical evidence on the interaction between the nonthermal plasma and catalyst can accelerate various applications such as catalyst preparation and regeneration, VOC removal, and chemical reforming processes at low temperature.

5. Conclusion

The influence of the Si/Al ratio on the interaction of plasma and Ag-supported HY zeolites was studied using multiple measurement techniques. The main findings in this study can be summarized as follows:

- (1) The oxidation stage of Ag was strongly influenced by the Si/Al ratio in the HY zeolites. The XPS data indicated that Ag became more oxidized at low Si/Al ratios and was in a metallic state at high Si/Al ratios. The electrical resistivity decreased rapidly as the Si/Al ratio of HY increased.
- (2) Metallic Ag exhibited a high catalytic activity for the thermal catalysis of benzene (i.e., without plasma application). Metallic Ag was also more effective for the decomposition of ozone than oxidized Ag, while the Ag^+ ion clusters contributed to ozone decomposition to a lesser extent.
- (3) The Si/Al ratio in the HY zeolite was an important factor for determining the catalytic activity under plasma activation. Propagation of surface streamers became less visible when the Si/Al ratio in the Ag/HY was above 15. The plasma-induced catalytic activity was closely related to the expansion of surface streamers on the zeolites. A higher catalytic activity was obtained using an HY zeolite with a lower Si/Al ratio, in which the surface streamers readily propagated on Ag/HY.
- (4) The ESR spectra of the plasma-treated Ag/HY zeolites indicated the formation of Ag^{2+} ions and Fe^{3+} ions. The formation of these new surface species was direct evidence of the surface modification by the plasma. The optical emission spectra confirmed the plasma-induced fluorescence from the Ag clusters incorporated in the framework of HY with relatively low Si/Al ratio.

The influence of Si/Al ratio in other types of zeolites is currently being studied, and will be reported separately.

Acknowledgement

The authors wish to acknowledge the financial support given by the Grant-in-aid for Scientific Research (C) (26400539).

References

- [1] E.C. Neyts, A. Bogaerts, *J. Phys. D: Appl. Phys.* 47 (2014) 224010.
- [2] F. Thevenet, L. Sivachandiran, O. Guaitella, C. Barakat, A. Rousseau, *J. Phys. D: Appl. Phys.* 47 (2014) 224011.
- [3] H.L. Chen, H.M. Lee, S.H. Chen, M.B. Chang, S.J. Yu, S.N. Li, *Environ. Sci. Technol.* 43 (2009) 2216–2227.
- [4] A.M. Vandenbroucke, R. Morent, N.D. Geyter, C. Leys, *J. Hazard. Mater.* 195 (2011) 30–54.
- [5] H.H. Kim, A. Ogata, *Eur. Phys. J.: Appl. Phys.* 55 (2011) 13806.
- [6] F. Holzer, F.D. Kopinke, U. Roland, *Plasma Chem. Plasma Process.* 25 (2005) 595–611.
- [7] C.L. Chang, T.S. Lin, *Plasma Chem. Plasma Process.* 25 (2005) 387–401.
- [8] M.K. Park, S.G. Ryu, H.B. Park, H.W. Lee, K.C. Hwang, C.H. Lee, *Plasma Chem. Plasma Process.* 24 (2004) 117–135.

- [9] M. Magureanu, N.B. Mandache, V.I. Parvulescu, C. Subrahmanyam, A. Renken, L. Kiwi-Minsker, *Appl. Catal. B: Environ.* 74 (2007) 270–277.
- [10] H.H. Kim, S.M. Oh, A. Ogata, S. Futamura, *J. Adv. Oxid. Technol.* 8 (2005) 226–233.
- [11] H.H. Kim, J.H. Kim, A. Ogata, *Int. J. Plasma Environ. Sci. Technol.* 2 (2008) 106–112.
- [12] H.H. Kim, A. Ogata, S. Futamura, *Appl. Catal. B: Environ.* 79 (2008) 356–367.
- [13] H.Y. Fan, X.S. Li, C. Shi, D.Z. Zhao, J.L. Liu, Y.X. Liu, A.M. Zhu, *Plasma Chem. Plasma Process.* 31 (2011) 799–810.
- [14] H.Y. Fan, C.S. Shi, X.S. Li, D.X. Zhao, Y. Xu, A.M. Zhu, *J. Phys. D: Appl. Phys.* 42 (2009) 225105.
- [15] Y.S. Mok, D.H. Kim, *Curr. Appl. Phys.* 11 (2011) S58–S62.
- [16] X. Dang, J. Huang, L. Cao, Y. Zhou, *Catal. Commun.* 40 (2013) 116–119.
- [17] D.Z. Zhao, X.S. Li, C. Shi, H.Y. Fan, A.M. Zhu, *Chem. Eng. Sci.* 66 (2011) 3922–3929.
- [18] A. Subrenat, J.N. Baléo, P.L. Cloirec, P.E. Blanc, *Carbon* 39 (2001) 707–716.
- [19] International Zeolite Association (IZA), <http://www.iza-structure.org/>
- [20] A. Ogata, D. Ito, K. Mizuno, S. Kushiya, T. Yamamoto, *IEEE Trans. Ind. Appl.* 37 (2001) 959–964.
- [21] S.M. Oh, H.H. Kim, H. Einaga, A. Ogata, S. Futamura, D.W. Park, *Thin Solid Films* 506–507 (2006) 418–422.
- [22] S.M. Oh, H.H. Kim, A. Ogata, H. Einaga, S. Futamura, D.W. Park, *Catal. Lett.* 99 (2005) 101–104.
- [23] T. Kuroki, K. Hirai, S. Matsuoka, J.Y. Kim, M. Okubo, *IEEE Trans. Ind. Appl.* 47 (2011) 1916–1921.
- [24] T. Kuroki, K. Hirai, R. Kawabata, M. Okubo, T. Yamamoto, *IEEE Trans. Ind. Appl.* 46 (2010) 672–679.
- [25] B. Eliasson, C.-J. Liu, U. Kogelschatz, *Ind. Eng. Chem. Res.* 39 (2000) 1221–1227.
- [26] K. Zhang, B. Eliasson, U. Kogelschatz, *Ind. Eng. Chem. Res.* 41 (2002) 1462–1468.
- [27] T. Jiang, Y. Li, C.-J. Liu, G.-H. Xue, B. Eliasson, B.-Z. Xue, *Catal. Today* 72 (2002) 229–235.
- [28] C. Liu, R. Mallinson, L. Lobban, *Appl. Catal. A: Gen.* 178 (1999) 17–27.
- [29] A. Yin, X. Guo, W.L. Dai, K. Fan, *J. Phys. Chem. C* 114 (2010).
- [30] S.M. Auerbach, K.A. Carrado, P.K. Dutta (Eds.), *Handbook of Zeolite Science and Technology*, Marcel Dekker Inc., New York, 2003.
- [31] H.H. Kim, S.M. Oh, A. Ogata, S. Futamura, *Catal. Lett.* 96 (2004) 189–194.
- [32] T. Sun, K. Seff, *Chem. Rev.* 94 (1994) 857–870.
- [33] N.D. Hutson, B.A. Reisner, R.T. Yang, B.H. Toby, *Chem. Mater.* 12 (2000) 3020–3031.
- [34] C.D. Wagner, W.M. Riggs, L.E. Davis, J.F. Mouider, G.E. Mullenberg, *Handbook of X-Ray Photoelectron Spectroscopy*, Perkin-Elmer Corporation Physical Electronics Division, MN, 1979.
- [35] L.H. Tjeng, M.B.J. Meinders, J.v. Elp, J. Ghijsen, G.A. Sawatzky, *Phys. Rev. B* 41 (1990) 3190–3199.
- [36] M. Jin, X. Zhang, S. Nishimoto, Z. Liu, D.A. Tryk, A.V. Emlene, T. Murakami, A. Fujishima, *J. Phys. Chem. C* 111 (2007) 658–665.
- [37] P. Prieto, V. Nistor, K. Nouneh, M. Oyama, M. Abd-Lefdil, R. Diaz, *Appl. Surf. Sci.* 258 (2012) 8807–8813.
- [38] Y. Lei, F. Mehmood, S. Lee, J. Greeley, B. Lee, S. Seifert, R.E. Winans, J.W. Elam, R.J. Meyer, P.C. Redfern, D. Teschner, R. Schogl, M.J. Pellin, L.A. Curtiss, S. Vajda, *Science* 328 (2010) 224–228.
- [39] Y. Kang, M. Sun, A. Li, *Catal. Lett.* 142 (2012) 1498–1504.
- [40] L. Jin, K. Qian, Z. Jiang, W. Huang, *J. Mol. Catal. A: Chem.* 274 (2007) 95–100.
- [41] S.-W. Baek, J.-R. Kim, S.-K. Ihm, *Catal. Today* 93–95 (2004) 575–581.
- [42] G. Corro, U. Pal, E. Ayala, E. Vidal, E. Guilleminot, *Top. Catal.* 56 (2013) 467–472.
- [43] T. Nanba, S. Masukawa, J. Uchisawa, A. Obuchi, *J. Catal.* 259 (2008) 250–259.
- [44] N. Kumar, P.M. Konova, A. Naydenov, Teemu, *Catal. Lett.* 98 (2004) 57–60.
- [45] M. Sugawara, A. Ogata, *Ozone Sci. Eng.* 33 (2011) 158–163.
- [46] X.D. Zhang, Z.P. Qu, X.Y. Li, M. Wen, X. Quan, D. Ma, J.J. Wu, *Sep. Purif. Technol.* 72 (2010) 395–400.
- [47] H. Fujita, J. Izumi, M. Sagehashi, T. Fujii, A. Sakoda, *Water Res.* 38 (2004) 166–172.
- [48] H.H. Kim, J.H. Kim, A. Ogata, *J. Phys. D: Appl. Phys.* 42 (2009) 135210.
- [49] A. Mizuno, Y. Yamazaki, S. Obama, E. Suzuki, K. Okazaki, *IEEE Trans. Ind. Appl.* 29 (1993) 262–267.
- [50] A. Mizuno, H. Ito, J. Electrostat. 25 (1990) 97–107.
- [51] A. Mizuno, Y. Yamazaki, H. Ito, H. Yoshida, *IEEE Trans. Ind. Appl.* 28 (1992) 535–540.
- [52] K. Takaki, J.S. Chang, K.G. Kostov, *IEEE Trans. Dielectr. Electr. Insul.* 11 (2004) 481–490.
- [53] M. Kuronen, H. Harjula, J. Jernstrom, M. Vestenius, J. Lehto, *Phys. Chem. Chem. Phys.* 2 (2000) 2655–2659.
- [54] Z. Li, M.C. Johnson, M. Sun, E.T. Ryan, D.J. Earl, W. Maichen, J.I. Martin, S. Li, C.M. Lew, J. Wang, M.W. Deem, M.E. Davis, Y. Yan, *Angew. Chem. Int. Ed.* 45 (2006) 6329–6332.
- [55] R.B. Clarkson, J.A.C. Cirillo, *J. Catal.* 33 (1974) 392–401.
- [56] P.H. Kasai, *J. Chem. Phys.* 43 (1965) 3322–3327.
- [57] N. Kanzaki, I. Yasumori, *J. Phys. Chem.* 82 (1978) 2351–2352.
- [58] A. Abou-Kais, J.C. Vedrine, C. Naccache, *J. Chem. Soc. Faraday Trans. II* 74 (1978) 959–967.
- [59] J. Michalik, A.v.d. Pol, E.J. Reijerse, T. Wasowicz, E.d. Boer, *Appl. Magn. Reson.* 3 (1992) 19–35.
- [60] Y. Akdogan, C. Vogt, M. Bauer, H. Bertagnolli, L. Giurgiu, E. Roduner, *Phys. Chem. Chem. Phys.* 10 (2008) 2952–2963.
- [61] R.A. Schoonheydt, H. Leeman, *J. Phys. Chem.* 93 (1989) 2048–2053.
- [62] Y. Teramoto, H.H. Kim, A. Ogata, N. Negishi, *IEEE Trans. Plasma Sci.* 32 (10) (2014) 2850–2851.
- [63] G.D. Cremer, E. Coutino-Gonzalez, M.B.J. Rooftaers, B. Moens, J. Ollevier, M.v.d. Auwerker, R. Schoonheydt, P.A. Jacobs, F.C.D. Schryver, J. Hofkens, D.E.d. Vos, B.F. Sels, T. Vosch, *J. Am. Chem. Soc.* 131 (2009) 3049–3056.
- [64] L.A. Peyser, A.E. Vinson, Andrew P. Bartko, R.M. Dickson, *Science* 291 (2001) 103–106.
- [65] M. Matsuoka, E. Matsuda, K. Tsuji, H. Yamashita, M. Anpo, *J. Mol. Catal. A: Chem.* 107 (1996) 399–403.
- [66] N. Herron, Y. Wang, M.M. Eddy, G.D. Stucky, D.E. Cox, K. Moller, T. Bein, *J. Am. Chem. Soc.* 111 (1989) 530–540.
- [67] J.L. Gole, R. Woodward, J.S. Hayden, D.A. Dixon, *J. Phys. Chem.* 89 (1985) 4905–4908.
- [68] T. Yamamoto, S. Takenaka, T. Tanaka, T. Baba, *J. Phys.: Conf. Ser.* 190 (2009) 012171.
- [69] H.H. Kim, A. Ogata, M. Schiorlin, E. Marotta, C. Paradisi, *Catal. Lett.* 141 (2011) 277–282.
- [70] Y. Teramoto, H.H. Kim, A. Ogata, N. Negishi, *Catal. Lett.* 143 (2013) 1374–1378.
- [71] J. Shibata, Y. Takada, A. Shichi, S. Satokawa, A. Satsuma, T. Hattori, *Appl. Catal. B: Environ.* 54 (2004) 137–144.
- [72] A. Ogata, H.H. Kim, S. Futamura, S. Kushiya, K. Mizuno, *Appl. Catal. B: Environ.* 53 (2004) 175–180.
- [73] C.J. Liu, J. Zou, K. Yu, D. Cheng, Y. Han, J. Zhan, C. Ratanatawanate, B.W.L. Jang, *Pure Appl. Chem.* 78 (2006) 1227–1238.
- [74] C.J. Liu, Y. Zhao, Y. Li, D.S. Zhang, Z. Chang, W.H. BU, *ACS Sustain. Chem. Eng.* 2 (2013) 3–13.